

# Spectral signatures of non-thermal baths in quantum thermalization

Ricardo Román-Ancheyta,<sup>1,\*</sup> Barış Çakmak,<sup>2</sup> and Özgür E. Müstecaplıoğlu<sup>3</sup>

<sup>1</sup>*Instituto Nacional de Astrofísica, Óptica y Electrónica, Calle Luis Enrique Erro 1, Sta. Ma. Tonantzintla, Puebla CP 72840, México*

<sup>2</sup>*College of Engineering and Natural Sciences, Bahçeşehir University, Beşiktaş, Istanbul 34353, Turkey*

<sup>3</sup>*Department of Physics, Koç University, İstanbul, Sarıyer, 34450, Turkey*

(Dated: October 1, 2022)

We show that certain coherences, termed as heat-exchange coherences, which contribute to the thermalization process of a quantum probe in a repeated interactions scheme, can be extracted from the power spectrum of the probe system. We suggest to use the power spectrum as a way to assess the apparent temperature of non-thermal atomic clusters carrying such coherences and also prove that it is useful to measure the corresponding thermalization time of the probe. We explore this idea in two examples in which the probe is assumed to be a single-qubit and a single-cavity field mode. Moreover, for the single-qubit case, we show how it is possible to perform a robust quantum simulation of resonance fluorescence using such repeated interactions scheme with clusters carrying different class of coherences.

## I. INTRODUCTION

In the rapidly growing field of quantum thermodynamics [1–3] several new effects that could bend the rules [4] of the classical theory are being predicted. Especially, developments related with the performance of non-thermal quantum machines constitute a good example to these effects, with which one can extend the limits dictated by the classical thermodynamics by exploiting the quantumness of the bath that the system of interest is interacting [5–17]. The distinguishing property of such non-thermal baths is that they possess some amount of quantum coherence, and as a result they can not be described by a thermal state. A natural question at this point would be to ask about the effects of the coherences in the bath on the dynamics of the central system while they are in contact. It has been shown that it is possible to fully characterize the types of coherences in a non-thermal bath. While some coherences have a displacing or squeezing effects, there are certain types of coherences that merely contribute to the thermalization of the system, which are dubbed as *heat-exchange coherences* (HECs) [7, 8, 13, 14]. Therefore, non-thermal baths that only contain HECs act as an effective heat bath for the probe, at a certain temperature depending on the actual values of the coherences.

How to assign an effective temperature to these non-thermal baths and how to test their corresponding quantum thermodynamic predictions from the spectroscopic point of view are the questions that lie at the heart of this contribution. We present a method that relies on the power spectrum of the probe system to assess the temperature of the bath for which it is possible to show that one can separately identify the effects of a thermal and a non-thermal, coherent bath. Moreover, the information about the thermalization time of the probe can

also be extracted from the power spectrum. The presented method is actually along the same lines with the recent efforts in quantum thermometry, which tries to estimate the temperature of an environment by quantum probes [18–27]. Specifically, the present approach resembles the one adopted in [23], in which the authors take advantage of the dephasing dynamics of a qubit that is embedded in an environment to assign a temperature to that environment. However, in this work, the environment with which the probe is interacting need not to be a thermal one and can contain certain coherences that appears as an effective temperature to the probe.

In particular, we generalize the previous settings presented in [7, 8, 13, 14] and consider a probe system that is both in contact with a thermal and a non-thermal bath that only contain HECs, and address the aforementioned matter of thermalization dynamics by considering two simple, but not trivial, examples in the weak coupling regime. We begin by considering a central single-qubit as our probe [see Fig. 1(a)] which is interacting randomly with a  $N$ -qubit coherent cluster (non-thermal bath) together with a thermal bath and derive some of their quantum thermodynamic effects on the probe, including the thermalization temperature and time. Then, we replace the qubit by a single electromagnetic field mode as our probe [see Fig. 1(b)], and we show that the effective field temperature is the same as the qubit case, however, their respective thermalization times are completely different. Interestingly, when coherences that are different from HECs are considered to be present in the  $N$ -qubit cluster, this scheme can also be used to perform a quantum simulation of resonance fluorescence in an ordinary or squeezed vacuum in free space.

The rest of the manuscript is organized as follows. In Sec. II, we introduce our model to manipulate the temperature of a quantum probe by interacting it with an  $N$ -qubit cluster that possess certain coherences. Sec. III presents our results on how to assess the temperature of the thermal bath and the apparent temperature of the coherent qubit clusters, and thermalization time of the

\* ancheyta6@gmail.com

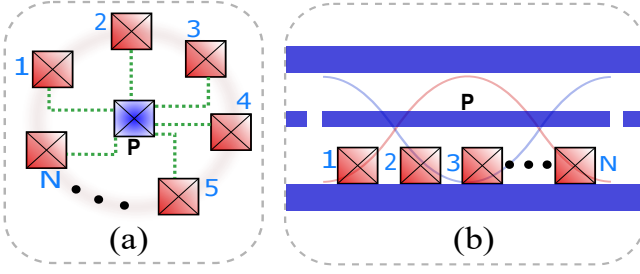


**FIG. 1.** (Color online) Schematic representations of a repeated interaction schemes also known as generalized micromaser setups. (a) A central probe qubit (blue central box) interacting randomly with a  $N$ -qubit coherent cluster (red surrounding boxes) acting as a non-thermal bath. (b) A single-electromagnetic field mode (blue thin rectangle) interacting randomly with a similar  $N$ -qubit cluster. These setups resemble the ones used in the field of circuit-QED, where boxes represent superconducting qubits and long rectangles are 1D transmission line resonators. However, setups based on cavity-QED architecture where an atomic cluster beam traverse a 3D electromagnetic cavity will also work.

quantum probe by looking at the stationary power spectrum of it. In Sec. IV, by adopting a time-dependent physical spectrum, we identify which types of coherences can be used to shape the spectral response of the qubit probe and make a quantum simulation of resonance fluorescence. We conclude in Sec. V.

## II. MODELS OF QUANTUM-THERMALIZING MACHINES

Throughout this section we present some properties of the thermalization dynamics associated with two non-thermal quantum machines subject to diverse dissipative and decohering processes. Similar results have also obtained by the authors in Ref. [8] in the absence of a thermal photon bath and decoherence. These properties shall be the basis and motivation for further study of the power spectrum associated with the probe in Sec. III and the respective characterization of them by means of spectroscopic measurements.

### A. Single qubit probe for an non-thermal bath of $N$ -qubit clusters

First, let us consider our central system as a single-qubit, with self-Hamiltonian  $H_q = \hbar\omega_q\sigma_z/2$  of frequency  $\omega_q$ , embedded in a thermal photon bath and also interacting *randomly* during a time “ $\tau$ ” at a rate  $p$  with an environment made of  $N$  identical qubits [see Fig. 1(a)] that we will call it the cluster  $H_{cl} = \sum_j \hbar\omega_q\sigma_z^j/2$ , through a dipolar interaction  $H_{dip} = \sum_j \hbar g(\sigma_+^j\sigma_- + \sigma_-^j\sigma_+)$ . Here,  $g$  is the interaction strength,  $\sigma_z^j$  and  $\sigma_\pm^j$  are the usual Pauli  $z$  and ladder operators of the  $j = 1, 2, \dots, N$ -th qubit, re-

spectively with  $[\sigma_z^i, \sigma_\pm^j] = \pm 2\sigma_\pm^i\delta_{ij}$  and  $[\sigma_+^i, \sigma_-^j] = \sigma_z^i\delta_{ij}$ . Without ambiguity, operators without superscript  $j$  will refer to the central qubit system. Following the approach adopted for the micromaser theory [28], we will assume that before each *random* interaction the state of the  $N$ -qubit cluster has to be reset to its initial state  $\rho_{cl}$ . Under this assumption, it is possible to derive a Markovian master equation for the single-qubit density matrix  $\rho_q$ . Thereby, tracing out the degrees of freedom of the cluster, in the interaction picture associated with the self Hamiltonian of the central qubit, and up to second order in  $g\tau$  we get (see Appendix A for a detailed derivation):

$$\dot{\rho}_q = r_d\mathcal{L}[\sigma_-]\rho_q + r_e\mathcal{L}[\sigma_+]\rho_q + \gamma_\phi\mathcal{L}[\sigma_z/4]\rho_q, \quad (1)$$

where  $\mathcal{L}[o]\rho_q \equiv 2o\rho_q o^\dagger - o^\dagger o\rho_q - \rho_q o^\dagger o$  is the usual Lindblad super-operator.  $r_e = [\mu_q\langle J_+J_- \rangle + \gamma\bar{n}_{en}]/2$  and  $r_d = [\mu_q\langle J_-J_+ \rangle + \gamma(\bar{n}_{en} + 1)]/2$  are the excitation (heating) and de-excitation (cooling) rates, respectively, with  $\mu_q = p(g\tau)^2$  is the effective coupling rate and  $\bar{n}_{en} = (\exp[\hbar\omega_q/(k_B T_{en})] - 1)^{-1}$  is the average photon number of a possibly unavoidable background thermal environment at temperature  $T_{en}$  that it is in contact with the central qubit system.  $J_\pm = \sum_j \sigma_\pm^j$  and  $J_z = \sum_j \sigma_z^j/2$  are the collective spin operators [29]. It is known that dissipation of energy and dephasing have a dramatic impact on the performance of quantum thermal and non-thermal machines. For instance, making use of dissipation in the photon field and pure atomic dephasing the quantum-classical transition of a photon-Carnot engine was evidenced in [11]. Here, those decoherence processes are incorporate, phenomenologically in Eq. (1), through the qubit spontaneous emission (SE) coefficient  $\gamma$  and a nonradiative dephasing rate  $\gamma_\phi$ .

Coherences of  $\rho_{cl}$  that contribute to the average value  $\langle J_-J_+ \rangle = \text{Tr}\{\rho_{cl}J_-J_+\}$  and its complex conjugate were identified as the HECs of the  $N$ -qubit cluster [8, 13, 14] which, in turn, act as an environment with an apparent temperature to the central qubit system. Therefore, along this work, we will be interested in determining  $\langle J_\pm J_\mp \rangle$  and their influence on the quantum evolution of the central system.

Equation (1) has the following solution for its density matrix elements [30]:

$$\rho_{eg}(t) = \rho_{eg}(0) \exp[-(r_d + r_e + \gamma_\phi)t], \quad (2a)$$

$$\rho_{ee}(t) = \frac{[r_d\rho_{ee}(0) - r_e\rho_{gg}(0)]e^{-2t(r_d+r_e)} + r_e}{r_d + r_e}, \quad (2b)$$

$\rho_{ge}(t) = \rho_{eg}(t)^*$  and  $\rho_{gg}(t) = 1 - \rho_{ee}(t)$ . We have used the notation  $\rho_{eg} = \langle e|\rho_q|g \rangle$ ,  $\rho_{ee} = \langle e|\rho_q|e \rangle$ ,  $\rho_{gg} = \langle g|\rho_q|g \rangle$  and  $\rho_{ge} = \langle g|\rho_q|e \rangle$ , where  $|g \rangle$  ( $|e \rangle$ ) is the ground (excited) qubit state. The qubit steady state  $\rho_q^{st}$  is a statistical mixture of its excited and ground states with probabilities  $\rho_{ee}^{st} = \rho_{ee}(\infty) = r_e/(r_d + r_e)$  and  $\rho_{gg}^{st} = \rho_{gg}(\infty) = r_d/(r_d + r_e)$  respectively. Assuming that  $\rho_q^{st}$  can be described by the Gibbs state  $\exp[-(\hbar\omega_q/(2k_B T_q))\sigma_z]$  we can have a well defined effective or apparent [31] qubit

temperature given by  $T_q = (\hbar\omega_q/k_B)\ln(r_d/r_e)^{-1}$  provided that  $r_d/r_e > 1$ . Hence, qubit temperature can be controlled by the ratio between the cooling and heating rates. Notice that at the end of the evolution  $T_q$  could also be obtained by looking for the population of the qubit excited steady state since  $T_q = (\hbar\omega_q/k_B)\ln(\rho_{ee}^{st}-1)^{-1}$ . From Eqs. (2a) and (2b), we see that  $\gamma_\phi$  only affects the off-diagonal density matrix elements, which implies that dephasing does not change either  $T_q$  or the qubit thermalization time  $t_q \equiv [2(r_d + r_e)]^{-1}$ . The latter can be rewritten as

$$t_q = \frac{1}{\gamma(2\bar{n}_{\text{en}} + 1) + 2\mu_q(\langle J^2 \rangle - \langle J_z^2 \rangle)}, \quad (3)$$

where  $J^2 = J_z^2 + (J_+J_- + J_-J_+)/2$  is the *Casimir* operator of  $\mathfrak{su}(2)$  [29].

### B. Single cavity probe for an non-thermal bath of $N$ -qubit clusters

Now we replace the single-qubit central system from the previous example by a single electromagnetic field mode  $H_c = \hbar\omega_c a^\dagger a$  of frequency  $\omega_c$  inside a leaky cavity. The resonance *random* interaction (of strength  $\lambda$ ) between the field and the  $N$ -qubit coherent clusters is governed by the Tavis-Cummings (TC) Hamiltonian  $H_{\text{TC}} = \lambda(J_+a + J_-a^\dagger)$  [32]. Here,  $a$  ( $a^\dagger$ ) is the usual annihilation (creation) bosonic field operator that satisfy  $[a, a^\dagger] = 1$ . In Ref. [33],  $H_{\text{TC}}$  has been realized experimentally (up to  $N = 3$  and later  $N = 8$  [34]) in the context of circuit-QED. A schematic representation of the TC model is sketched in Fig. 1(b). Under the standard assumptions of the micromaser theory [28, 35] and within afore-mentioned conditions, the following Markovian master equation for the electromagnetic field density matrix  $\rho_c$  (in a rotating frame at the cavity frequency) can be derived [13, 36] (see Appendix A):

$$\dot{\rho}_c = \mathcal{R}_d \mathcal{L}[a]\rho_c + \mathcal{R}_e \mathcal{L}[a^\dagger]\rho_c + \kappa_\phi \mathcal{L}[a^\dagger a]\rho_c, \quad (4)$$

Once again,  $\mathcal{R}_d = [\mu_c \langle J_- J_+ \rangle + \kappa(\bar{n}_{\text{en}} + 1)]/2$  and  $\mathcal{R}_e = [\mu_c \langle J_+ J_- \rangle + \kappa\bar{n}_{\text{en}}]/2$  represent the cooling and heating rates respectively.  $\kappa$  ( $\kappa_\phi$ ) is the cavity field decay (dephasing) rate and  $\bar{n}_{\text{en}}$  now depends on the  $\omega_c$  instead of  $\omega_q$ . Like in the previous case  $\mu_c = p(\lambda\tau)$  is the effective coupling rate. To elucidate how the HECs intervene in the cavity field evolution, we first calculate the corresponding equations of motion for the photon number  $a^\dagger a$  and field  $a$  operators, these are given by  $\langle a^\dagger a \rangle_t = -2(\mathcal{R}_d - \mathcal{R}_e)\langle a^\dagger a \rangle_t + 2\mathcal{R}_e$  and  $\langle \dot{a} \rangle_t = -(\mathcal{R}_d - \mathcal{R}_e + \kappa_\phi)\langle a \rangle_t$ . The notation  $\langle \mathcal{O} \rangle_t = \text{Tr}\{\rho_c \mathcal{O}(t)\}$  was used. Taking the initial conditions  $\langle a^\dagger a \rangle_0$  and  $\langle a \rangle_0$  their solutions are:  $\langle a^\dagger a \rangle_t = n_{st} + (\langle a^\dagger a \rangle_0 - n_{st})\exp[-2(\mathcal{R}_d - \mathcal{R}_e)t]$  and  $\langle a \rangle_t = \langle a \rangle_0 \exp[-(\mathcal{R}_d - \mathcal{R}_e + \kappa_\phi)t]$ , where  $n_{st} = \mathcal{R}_e(\mathcal{R}_d - \mathcal{R}_e)^{-1}$  is the steady state photon number. Substituting the values of the excitation and de-excitation rates yields  $n_{st} = (\kappa\bar{n}_{\text{en}} + \mu_c \langle J_+ J_- \rangle) / (\kappa - 2\mu_c \langle J_z \rangle)$ . As

in the previous single-qubit probe case we assume that the steady state of the field can be described by a thermal state  $\exp[-(\hbar\omega_c/k_B T_c)a^\dagger a]$  with an associated effective temperature [31] given by  $T_c = (\hbar\omega_c/k_B)\ln(\mathcal{R}_d/\mathcal{R}_e)^{-1}$ , which turns out to be  $T_c = (\hbar\omega_c/k_B)\ln(n_{st}^{-1} + 1)^{-1}$ . On the other hand, thermalization time of the field mode is given by  $t_c \equiv [2(\mathcal{R}_d - \mathcal{R}_e)]^{-1}$ , which can be rewritten in terms of the total population inversion  $\langle J_z \rangle$  as:

$$t_c = \frac{1}{\kappa - 2\mu_c \langle J_z \rangle}. \quad (5)$$

The interaction of the central system with the  $N$ -qubit coherent cluster can modify its natural (or fabricated) parameters. For instance, from Eq. (5) it is clear that the coherence time of the field mode can be enhanced just by having, for example, a large number of environmental qubits in their excited state, this could improve the performance of a thermal machine using the field mode as the probe. Such a situation is especially useful when changing the quality factor of a cavity (or transmission line resonator) is difficult due to manufacturing limitations.

### C. Bath size effects on the probe thermalization

So far, we can point out some important things regarding thermalization of the single-qubit system and the single-field mode. Despite the fact that  $T_q$  and  $T_c$  look different, they are defined as the logarithm of the ratio between their respective *heating* and *cooling* rates. Consequently, both temperatures have the same dependency on  $\langle J_\pm J_\mp \rangle$ . This implies that the only difference between both temperatures should be attributed to the corresponding parameters that characterize each physical system. However, there must be some situations, of practical purposes, in which it would be more advantageous to work with a cavity field mode (resonator) instead of a single-qubit as the main central system or vice versa. As an example, let's consider the initial state of  $N$ -qubit cluster to be a Dicke state  $\rho_{\text{cl}} = |k, N\rangle\langle k, N|$ . This is a non-thermal state prepared by non-thermal means where  $k$  is the number of excitations in the cluster and  $\langle J_+ J_- \rangle = k(N - k + 1)$ ,  $\langle J_- J_+ \rangle = (k + 1)(N - k + 1)$  and  $\langle J_\pm \rangle = \langle J_\pm^2 \rangle = 0$  [37]. It is easy to prove that  $T_q$  and  $T_c$  grow with  $N^2$  (superlinear scaling behavior), but the corresponding thermalization times are quite different,  $t_q$  is inversely proportional to  $N^2$  and  $t_c$  is independent of the number of environmental qubits, providing that  $k = N/2 - 1$  [8]. Hence, if there is a difference between the thermalization time of a bosonic and fermionic probes, this should be relevant for the design of future quantum thermal and non-thermal machines. For instance, any shortening in  $t_q$  or  $t_c$  could be used to boost the performance of a quantum heat engine operating at a finite time [38]. Therefore, it is necessary to know how to check this behavior experimentally, in Sec. III we will address this question from the spectroscopic point of view.

### D. Case study: $N=2$ qubit cluster

The results obtained in the previous section are quite general. In order to clearly demonstrate these results, which shows a transparent link between the HECs and these quantum thermalization effects, we now choose a specific size for the coherent cluster,  $N = 2$ , with the following initial state (written in the standard two-qubit basis  $[ee, eg, ge, gg]$ )

$$\rho_{\text{cl}}(\phi, \zeta) = \begin{pmatrix} 0 & 0 & 0 & 0 \\ 0 & \sin^2 \phi & \zeta \sin \phi \cos \phi & 0 \\ 0 & \zeta^* \sin \phi \cos \phi & \cos^2 \phi & 0 \\ 0 & 0 & 0 & 0 \end{pmatrix}, \quad (6)$$

where  $\zeta$  is a kind of purity parameter such that  $|\zeta| \leq 1$  and  $\phi \in [-\pi/4, \pi/4]$ . For  $\zeta=0$  ( $\zeta=1$ ) the Eq. (6) reduce to a statistical mixture (Bell-like state). Without loss of generality, we have assumed  $\zeta$  to be a non-negative real number. This state will help us to make the connection between the HECs and the properties of the power spectrum of the probe system in the next section, Sec. III. Accordingly,  $\rho_{\text{cl}}(\phi, \zeta)$  gives the following result for the expectation values

$$\langle J_{\pm} J_{\mp} \rangle = 1 + 2\zeta \sin \phi \cos \phi, \quad (7)$$

and  $\langle J_{\pm} \rangle = \langle J_{\mp}^2 \rangle = 0$ . We identify the off-diagonal terms  $\zeta \sin \phi \cos \phi$  of  $\rho_{\text{cl}}(\phi, \zeta)$  as the so called HECs since they contribute to the *heating* and *cooling* rates through Eq. (7). First, we proceed to examine their action on the probe temperature. From the discussion in Sec.s II A and II B, we know that the thermalization temperatures of both qubit ( $T_q$ ) and cavity ( $T_c$ ) probe are the same. Therefore, we decided to exemplify the HEC dependence of final temperature by working with a cavity probe. Using Eq. (6), we find  $\langle J_z \rangle = 0$  and the steady state photon number reads as  $n_{st} = \bar{n}_{\text{en}} + (\mu_c/\kappa)(1 + \zeta \sin 2\phi)$ . Thus, any change in  $n_{st}$  due to  $\zeta$  or  $\phi$  will be reflected directly in  $T_c$ . This can be seen in Fig. 2, where we show how the ratio of the final temperature of the cavity to the thermal environment temperature,  $T_c/T_{\text{en}}$ , and HECs, change as a function of  $\phi$  for different values of  $\zeta$  and relative interaction strength  $\mu_c/\kappa$ . In fact, Fig. 2 demonstrates how  $T_c$  differs, as expected [13], when the interaction with the  $N$ -qubit coherent cluster is on as compared to the case where only thermal bath and incoherent clusters are present (dotted lines). In addition, depending on the sign of coherences of  $\rho_{\text{cl}}(\phi, \zeta)$  it is possible to heat (cool) the probe above (below) the temperature of the thermal bath with maximum attained when  $\phi = \pi/4$  ( $-\pi/4$ ) for a given value of  $\zeta$ .

In contrast to final temperatures, thermalization times are distinct when again  $\rho_{\text{cl}}(\phi, \zeta)$  is considered as the non-thermal bath. Specifically, Eq. (5) reduces to  $t_c^{-1} = \kappa$  and Eq. (3) to  $t_q^{-1} = \gamma(1 + 2\bar{n}_{\text{en}}) + 2\mu_q(1 + \zeta \sin 2\phi)$ , due to  $\langle J^2 \rangle - \langle J_z^2 \rangle = 1 + \zeta \sin 2\phi$  for the latter case.

Before, moving on to the next section, we would like make a small comment on the correlation and coherence

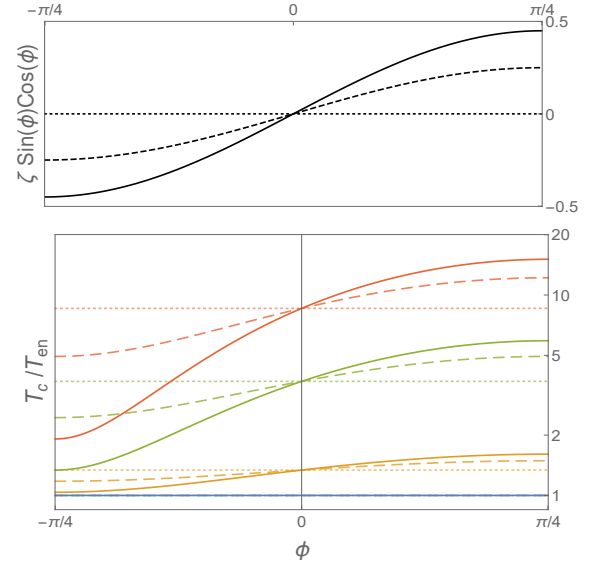


**FIG. 2.** (Color online) Above: HEC of the state (6) as a function of  $\phi$  for purity parameter  $\zeta = \{0.9, 0.5, 0\}$  (solid, dashed, dotted). Below: ratio between cavity field temperature  $T_c$  and the temperature of its local environment at  $T_{\text{en}}$ . Relative interaction strength  $\mu_c/\kappa = \{0, 0.1, 1, 3\}$  (blue, orange, green, red). Average thermal photon number is  $\bar{n}_{\text{en}} = 0.1$ , which could correspond to  $T_{\text{en}} \sim \text{mK}$  ( $\sim 298 \text{ K}$ ) at microwave (optical) frequencies.

properties of considered coherent cluster state. The entanglement content of Eq. (7), as quantified by the concurrence [39], can be found as  $\mathcal{C} = 2\zeta |\sin \phi \cos \phi|$ . In the present case the entanglement of the cluster turns out to be equal to the  $l_1$ -norm of coherence [40], which is defined as the sum of absolute values of all off-diagonal elements of the state. Therefore, it is possible to conclude that these quantities actually have a direct effect in the final temperatures of the probes. Although broad temperature control in cavities by combustion of two-atom entanglement has already been predicted in [7]; in this work, we have extended the validity of those results for the case in which the probe can be of a fermionic nature. More importantly, we have showed that these different cases yield completely different thermalization times for the same amount of coherences in the non-thermal environment.

### III. SPECTRAL MEASUREMENTS

Up to this point, we have verified that changes in the parameters controlling the HECs or in the size of the cluster have a direct impact on the temperature and thermalization time of the corresponding probe. Now, we present a way to experimentally test such predictions. In this section, we will address such an inquiry using the power spectrum of the probe.



### Stationary power spectrum

The stationary (Wiener-Khintchine) power spectrum [41, 42] associated with the single-qubit probe, is defined as [43, 44]:

$$S_q(\omega) = \frac{1}{\pi} \text{Re} \int_0^\infty d\tau e^{i\omega\tau} \langle \sigma_+(0) \sigma_-(\tau) \rangle, \quad (8)$$

where  $\langle \sigma_+(0) \sigma_-(\tau) \rangle = \lim_{t \rightarrow \infty} \langle \sigma_+(t) \sigma_-(t + \tau) \rangle$  is the first order dipole-field auto-correlation function. In the steady state of the system at hand, it can be calculated as (see Appendix B):  $\langle \sigma_+(0) \sigma_-(\tau) \rangle = \rho_{ee}^{st} \exp[-(i\omega_q + \gamma_\phi + (2t_q)^{-1})\tau]$ . Using this result, we can perform the integral in Eq. (8) and obtain the stationary power spectrum of the qubit as follows

$$S_q(\omega) = \frac{\rho_{ee}^{st}}{\pi} \frac{\frac{1}{2}\Gamma_q}{(\omega - \omega_q)^2 + (\frac{1}{2}\Gamma_q)^2}, \quad (9)$$

which is a Lorentzian peak of full width at half maximum (FWHM) given by  $\Gamma_q = 2\gamma_\phi + t_q^{-1}$ . Further, we can use Eq. (3) to replace the thermalization time and obtain

$$\Gamma_q = 2\gamma_\phi + \gamma(2\bar{n}_{\text{en}} + 1) + 2\mu_q(\langle J^2 \rangle - \langle J_z^2 \rangle). \quad (10)$$

$S_q(\omega)$  has a maximum at  $\omega_q$  given by  $2\rho_{ee}^{st}/(\Gamma_q\pi)$ . The intensity can be calculated as the integral over all frequencies  $I_q \equiv \int_{-\infty}^\infty S_q(\omega) d\omega = \rho_{ee}^{st}$ .

On the other hand, the power spectrum of the single-field mode is defined as

$$S_c(\omega) = \frac{1}{\pi} \text{Re} \int_0^\infty d\tau e^{i\omega\tau} \langle a^\dagger(0) a(\tau) \rangle, \quad (11)$$

and if we repeat the same procedure as we did for the qubit case, it is possible to find the power spectrum as

$$S_c(\omega) = \frac{n_{st}}{\pi} \frac{\frac{1}{2}\Gamma_c}{(\omega - \omega_c)^2 + (\frac{1}{2}\Gamma_c)^2}, \quad (12)$$

with its maximum and spectral bandwidth being  $S_c(\omega_c) = 2n_{st}/(\Gamma_c\pi)$  and  $\Gamma_c = 2\kappa_\phi + t_c^{-1}$ , respectively. Again, similar to the qubit case, we can substitute the thermalization time of the cavity from Eq. (5) to obtain

$$\Gamma_c = 2\kappa_\phi + \kappa - 2\mu_c \langle J_z \rangle, \quad (13)$$

resulting in a cavity intensity of  $I_c \equiv \int_{-\infty}^\infty S_c(\omega) d\omega = n_{st}$ . We observe that in both cases the spectral bandwidth depends explicitly on the corresponding thermalization times. Hence, by measuring the FWHM of these spectral signals, it is possible to infer how fast or slow is the thermalization process. Moreover, measuring their intensity (signal integration) one can obtain the temperature that has been reached by the probe.

If we rewrite the ratio  $r_d/r_e$  ( $\mathcal{R}_d/\mathcal{R}_e$ ) and the sum (difference)  $r_d + r_e$  ( $\mathcal{R}_d - \mathcal{R}_e$ ) in terms of  $I_q$  ( $I_c$ ) and

$\Gamma_q$  ( $\Gamma_c$ ) respectively, we can arrange simple and general expressions for the average values we are interested in:

$$\langle J_+ J_- \rangle = (\Gamma_p - 2\gamma_p^\phi)(I_p)\mu_p^{-1} - \frac{\gamma_p}{\mu_p} \bar{n}_{\text{en}}, \quad (14a)$$

$$\langle J_- J_+ \rangle = (\Gamma_p - 2\gamma_p^\phi)(1 \pm I_p)\mu_p^{-1} - \frac{\gamma_p}{\mu_p} (1 + \bar{n}_{\text{en}}), \quad (14b)$$

where the subscript “p” specify the type of the probe, i.e.,  $q$  or  $c$ . In the same manner, decay rate  $\gamma_p$  ( $\gamma_p^\phi$ ) must be replaced by  $\gamma$  or  $\kappa$  ( $\gamma_\phi$  or  $\kappa_\phi$ ). The change of sign in Eq. (14b) comes from considering the single-qubit instead of the cavity mode as the central system. Eqs. (14) are useful because they enable us to establish a link between spectroscopic parameters,  $\Gamma_p$  and  $I_p$  and HECs, therefore provide the information on whether or not HECs are present in the environment that our probe system is interacting. As the collective spin correlators carry information on the multipartite coherences and entanglement among the environment qubits, our results could allow for spectroscopic quantum thermometry of quantum correlations in a non-thermal environment that can be associated with an apparent temperature. In the following subsection, we will elaborate on these results.

### Heat exchange coherences in the power spectrum

Now we use the spectra of Eqs. (9) and (12) to show how it is possible to differentiate between states of the  $N$ -qubit cluster having HECs from those who are a statistical mixture. For clarity we consider again the state described by Eq. (6) as an example, from Eq. (10) follows

$$\Gamma_q = 2\gamma_\phi + \gamma(2\bar{n}_{\text{en}} + 1) + 2\mu_q(1 + \zeta \sin 2\phi). \quad (15)$$

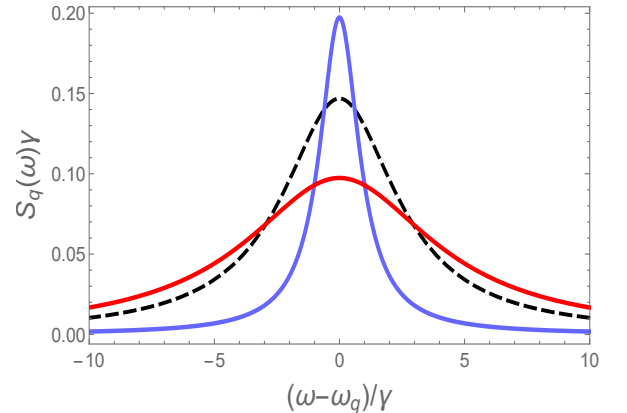


**FIG. 3.** (Color online) Power spectrum of the single-qubit probe [see Eq. (9)] when the initial state of the environmental cluster is the Eq. (6). Black dashed line is for  $\zeta = 0$  (mix state). Solid lines are for  $\zeta = 0.9$  (state with HECs) and  $\phi = \{-\pi/4, \pi/4\}$  (blue, red) represent, respectively, the coldest and hottest effective qubit temperature for this value of  $\zeta$ . We set  $\mu_q = 2\gamma$ ,  $\gamma_\phi = 0.15\gamma$  and  $\bar{n}_{\text{en}} = 0.1$ . The spectral bandwidth and the amplitude have a strong dependency on  $\zeta$  and  $\phi$ .

The inclusion of HECs in Eq. (6) will (depending on the sign of  $\sin 2\phi$ ) increase or decrease the spectral bandwidth by an amount  $\Delta\Gamma_q \equiv \Gamma_q - \Gamma'_q = 2\zeta\mu_q \sin 2\phi$ , where  $\Gamma'_q$  is the FWHM of the mix state  $\rho_{cl}(\phi, 0)$ . The increase (decrease) is maximum when  $\zeta = 1$  and  $\phi = \pi/4$  ( $-\pi/4$ ). For  $\phi = -\pi/4$  the bandwidth can even be equal to the natural (or fabricated) spectral linewidth of the qubit as long as  $\gamma_\phi$  and  $\bar{n}_{en}$  are negligible. This behavior is shown in Fig. 3 where amplitude variations also can be observed. For the field mode case we cannot apply previous spectral bandwidth analysis when using Eq. (6) because  $\langle J_z \rangle = 0$  and  $\Gamma_c = 2\kappa_\phi + \kappa$  remains as if there had not been an interaction with the  $N$ -qubit cluster. However, signatures of HECs in  $S_c(\omega)$  still can be found, these are encoded in the field intensity given by  $I_c = \bar{n}_{en} + (\mu_c/\kappa)(1 + \zeta \sin 2\phi)$ . Note that in both cases, HECs affect the same spectral parameters that the temperature of the thermal environment affects. This is in line with our claims that HECs only contribute to the heat flow between the interacting quantum probe and non-thermal environment but cannot be transferred as coherence. All in all, it is nice to see this verification in experimentally accessible spectroscopic parameters.

On the other hand, if the cluster is initially in the Dicke state  $|k, N\rangle$  with  $k = N/2 - 1$ , then the bandwidth of the single-qubit central system depends quadratically on  $N$ :

$$\Gamma_{\text{Dicke}} = 2\gamma_\phi + \gamma(2\bar{n}_{en} + 1) + \mu_q(N + N^2/2 - 2). \quad (16)$$

Thus, in this case, given a set of values  $\{\gamma_\phi, \gamma, \bar{n}_{en}\}$  there should be a critical number of qubits in the cluster in order to be more significant than contributions of the dissipation and/or dephasing rate. In other words, the control of the spectral bandwidth is imposed by changes of the cluster size.

These results indicate that we are capable of discriminating between a quantum non-thermal machine operating with a bath containing HECs, from a thermal machine in which its environment is in a mixed state. Even more, we can know if the associated probe temperature is increasing or decreasing together with its rate, just by looking at the spectral properties it. In fact, presented approach is quite similar to the one put forward in [23], in which the authors suggest to assess the temperature of an environment by looking at the dephasing dynamics of a single, probe qubit that is in contact with that environment. In other words, even though the type of the environment and the interaction with the probe qubit is quite different in the model we consider as compared to [23], the power spectrum of the probe can be used in the same spirit, that is, to estimate the temperature of its environment. However, in this work, the environment that the probe qubit is in contact with do not need to be a thermal one, it can also be a non-thermal, coherent one that dictates an apparent temperature to the probe, through HECs.

#### IV. DISPLACEMENT COHERENCES IN THE POWER SPECTRUM

We now want to shift our attention from HECs to the different class of coherences in  $\rho_{cl}$  and analyze their effect on the power spectrum of the single qubit probe. In particular, we present how it is possible to shape the spectrum using the so called *displacement coherences* (DCs) [8], which are the matrix elements of  $\rho_{cl}$  that contribute to the expectation values  $\langle J_\pm \rangle$  [13, 14]. Under the assumptions outlined in Sec. II A, we can obtain an equation that rules the evolution of the single qubit probe assuming that only DCs are present in the coherent atomic cluster. Up to second order in  $gt$  the equation describing the dynamics reads as (see Appendix A for details):

$$\dot{\rho}_q = -i[H_{\text{eff}}, \rho_q], \quad (17)$$

where

$$H_{\text{eff}} = \tilde{\mu}\langle J_+ \rangle \sigma_- + \tilde{\mu}\langle J_- \rangle \sigma_+ \quad (18)$$

is the effective Hamiltonian. Note that  $H_{\text{eff}}$  emulates the semi-classical radiation-matter interaction between a two-level atomic system and a classical electric field. It is possible to identify an effective Rabi frequency given by  $\Omega_{\text{eff}} = 2\tilde{\mu}|\langle J_\pm \rangle|$  with  $\tilde{\mu} = pgt$ . In order to clearly and explicitly present the action of DCs on the spectrum of the qubit probe, we set  $\gamma = \gamma_\phi = \bar{n}_{en} = 0$ ,  $\langle J_\pm^2 \rangle = \langle J_\pm J_\mp \rangle = 0$ , and keep only  $\langle J_\pm \rangle \neq 0$  which guarantees that atomic bath clusters contain only DCs.

Since Eq. (17) describes unitary evolution of the system, it does not present a steady-state solution and thus we cannot make use of the quantum-regression formula to compute the dipole-field autocorrelation function. Therefore, it is not possible to calculate the idealized stationary power spectrum definition presented in Eq. (8). Instead, we will use the physical spectrum introduced by Eberly and Wódkiewicz (EW) [45]. In general, this spectrum definition can be applied to non-stationary light sources. For the single qubit probe it is defined as:

$$S(\omega, t, \Gamma_f) = 2\Gamma_f \int_0^t dt_1 \int_0^t dt_2 e^{-(\Gamma_f - i\omega)(t - t_1)} \times e^{-(\Gamma_f + i\omega)(t - t_2)} \langle \sigma_+(t_1) \sigma_-(t_2) \rangle, \quad (19)$$

where  $\omega$  and  $\Gamma_f$  are the central frequency and band half-width of a Fabry-Pérot cavity acting as a filter, respectively, and we assume its central line matches the qubit frequency  $\omega_q$ . The EW-spectrum is more realistic, it reduces to the previously introduced definition by Wiener-Khinchine for the stationary state,  $t \rightarrow \infty$ , and in the limit of infinite resolution,  $\Gamma_f \rightarrow 0$  [45]. If the qubit probe is initially in its ground state the dipole-field autocorrelation function is easily obtained [see Eq. (B2)], and

we can use it to express Eq. (19) in following way

$$S(\omega, t, \Gamma_f) = \frac{\Gamma}{2} e^{-2\Gamma_f t} \left\{ \left| \int_0^t d\tau e^{(\Gamma_f - i\omega)\tau} \sin(\Omega_{\text{eff}}\tau) \right|^2 + \left| \int_0^t d\tau e^{(\Gamma_f - i\omega)\tau} [1 - \cos(\Omega_{\text{eff}}\tau)] \right|^2 \right\}. \quad (20)$$

Analytical solution for the integrals of Eq. (20) is possible, however, the entire expression of the full time-dependent spectrum is too cumbersome to show here. Instead, a good approximate time-independent expression can be obtained in the long-time limit ( $t \gg 1$ ) [46], where after a few Rabi oscillations the spectrum has stabilized to three nearby Lorentzians:

$$S(\omega, \Gamma_f) = \frac{\frac{1}{4}\Gamma_f}{\Gamma_f^2 + [(\omega - \omega_q) + \Omega_{\text{eff}}]^2} + \frac{\frac{1}{2}\Gamma_f}{\Gamma_f^2 + (\omega - \omega_q)^2} + \frac{\frac{1}{4}\Gamma_f}{\Gamma_f^2 + [(\omega - \omega_q) - \Omega_{\text{eff}}]^2}. \quad (21)$$

A Mollow-like structure [47] can be inferred from above expression and its explicit behavior is shown in Fig. 4, where the satellite peaks are located at  $\omega = \omega_q \pm \Omega_{\text{eff}}$ . Recall that  $\Omega_{\text{eff}}$  is directly proportional to  $\langle J_{\pm} \rangle$ , therefore the magnitude of the DCs defines if the single qubit probe is in the weak, moderate or strong (where the sidebands emerge) driven regime. If we add energy losses into our system, we will be simulating the physical process of resonance fluorescence (RF) with an exact Mollow spectrum as a final result [47]. Such a setting can be created within the framework of the model we present in this work, if we assume that all different types of coherences are present in the bath, i.e.  $\langle J_{\pm} \rangle$ ,  $\langle J_{\pm}^2 \rangle$  and  $\langle J_{\pm} J_{\mp} \rangle$  are different from zero. Then, we could perform the quantum simulation of RF from a single two-level system in an artificial squeezed vacuum by a repeated interaction scheme. This scheme generates an effective Markovian master equation (A5) identical to that of a driven two-level atom in a squeezed vacuum in free space, without the necessity to use sources of true squeezed light. As the scheme consists of only qubit-qubit interactions it can provide arbitrarily strong squeezing [13]. Therefore, this is a viable alternative to control polarization decay and spectral response of a single qubit probe.

In addition to spectrum engineering and longevity of quantum coherence, these results can be significant for spectral characterization of unknown quantum resources for their quantum information and energy resource values as well. From the quantum thermodynamic point of view, the emergence of a Mollow-like triplet in the spectroscopy of the corresponding qubit probe should be considered as a strong signature of the system acting as a thermo-mechanical engine, such that the interaction with the non-thermal bath result in both heat and work to be imparted to the probe [13].

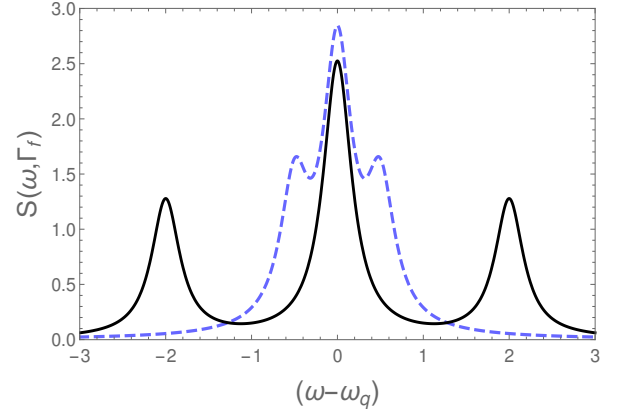


**FIG. 4.** Spectrum the the single qubit probe (21) when displacement coherences of the  $N$ -qubit cluster are taken into account. The displacement coherences,  $\langle J_{\pm} \rangle$ , define the location of the sidebands in this Mollow-like spectrum. We have set the effective Rabi frequency  $\Omega_{\text{eff}} \equiv 2\tilde{\mu}|\langle J_{\pm} \rangle|$  equals to 2 (black solid line) and 1/2 (blue dashed line).  $\Gamma_f = 0.2$ .

## V. CONCLUSIONS

We have studied the thermalization dynamics of two different types of quantum probes that are in contact with a thermal and non-thermal, coherent bath. We have modeled our quantum probes as a single-qubit and a single-mode cavity field, and showed the non-trivial effects of the coherences contained in the non-thermal bath (HECs) on the thermalization temperature and time of these model systems. We have proposed a strategy to measure these effects by investigating the power spectrum of the probes in both cases, and proved that the spectral bandwidth and intensity are explicitly dependent on HECs. Therefore, the suggested method is capable of identifying the apparent temperature of a non-thermal bath with HECs, as well as the temperature of a thermal bath, in spectroscopic experiments. We think that these results also contribute to the field of quantum thermometry which aims to estimate the temperature of an environment using a quantum probe. The presented spectroscopic method is not only capable of assessing the temperature of a thermal bath, but also points a direction on how to identify the effective temperature that a quantum probe sees when in contact with an non-thermal environment with only thermalizing coherences. Through such an apparent temperature, quantum thermometry of multipartite coherences and correlations could be possible for non-thermal environments. Another application of this method is the implementation of robust quantum simulation of resonance fluorescence using different types of coherences in the non-thermal bath. On top of being an significant result per se, observation of such an effect can again serve as a tool for characterizing an unknown environment via a single-qubit probe.

## ACKNOWLEDGMENTS

Ö. E. M. acknowledges support by TUBITAK (Grant No. 116F303) and by the EU-COST Action (CA15220).

### Appendix A: Generalized micromaser like equation

We make the derivation, following closely Ref. [12], of the micromaser master like equation used in Eqs. (1) and (4) of the main text. We start by considering a *random* “multipulse” type interaction between a central system  $S$  and a bath system  $B$  that is described by the linear coupling Hamiltonian  $H_I = \epsilon(B^\dagger s + Bs^\dagger)$ , where  $s, s^\dagger$  ( $B, B^\dagger$ ) are the annihilation and creation, central (bath) system operators respectively;  $\epsilon$  is the coupling coefficient. The corresponding evolution operator is  $U(\tau) = \exp(-iH_I\tau)$ . Before each interaction at time  $t_j$ , it is assumed that the state of the bath system  $B$  is reset to its initial value which does not have any correlation with  $S$ , so the total state is  $\rho(t_j) = \rho_s(t_j) \otimes \rho_B(0)$ . This assumption seems arbitrary, but actually, it is a typical physical situation in one-atom masers [28] for which, individual and independent Rydberg atoms pass one by one through a high-finesse electromagnetic cavity [48–50]. After each *random* interaction of duration  $\tau$ , the central system density matrix is  $\rho_s(t_j + \tau) = \text{Tr}_B\{U(\tau)\rho(t_j)U^\dagger(\tau)\}$ . If we introduce a rate  $p$  of a Poisson process to portray this *random* interaction, then in a time interval  $(t + \delta t)$  the probability of interaction will be  $p\delta t$ . As a consequence the state of the central system  $S$  can be written during this time interval as the sum of the two possible outcomes  $\rho_s(t + \delta t) = p\delta t \text{Tr}_B\{U(\tau)\rho(t)U^\dagger(\tau)\} + (1 - p\delta t)\rho_s(t)$ , where  $1 - p\delta t$  is the probability of having a non interaction event. If we divided the above equation by  $\delta t$  and take the limit when it goes to zero, we obtain the following differential equation for the central system density matrix

$$\dot{\rho}_s(t) = p[\text{Tr}_B\{U(\tau)\rho_s(t) \otimes \rho_B(0)U^\dagger(\tau)\} - \rho_s(t)], \quad (\text{A1})$$

where we have used the derivative definition:  $d\rho_s(t)/dt \equiv \lim_{\delta t \rightarrow 0} (\rho_s(t + \delta t) - \rho_s(t))/\delta t$ . By now (A1) is valid for any coupling strength and interaction time, however, in micromaser setups the product  $\epsilon\tau$  is normally small [12]. We proceed to approximate the evolution operator up second order in  $\epsilon\tau$  as:  $U(\tau) \sim 1 - U_1(\tau) - U_2(\tau)$ , where

$$U_1(\tau) = i\epsilon\tau(B^\dagger s + Bs^\dagger), \quad (\text{A2})$$

$$U_2(\tau) = (\epsilon\tau)^2(B^\dagger s + Bs^\dagger)^2/2. \quad (\text{A3})$$

Inserting (A2), (A3) in (A1), it yields

$$\begin{aligned} \dot{\rho}_s(t) = & p\text{Tr}_B\{U_1(\tau)\rho(t)U_1^\dagger(\tau) - U_1(\tau)\rho(t) \\ & - \rho(t)U_1^\dagger(\tau) - U_2(\tau)\rho(t) - \rho(t)U_2^\dagger(\tau)\}, \end{aligned} \quad (\text{A4})$$

where we have kept only terms up second order in  $\epsilon\tau$  neglecting  $U_1(\tau)\rho(t)U_2^\dagger(\tau) \propto (\epsilon\tau)^3$ ,  $U_2(\tau)\rho(t)U_2^\dagger(\tau) \propto (\epsilon\tau)^4$  and their complex conjugates. Hereafter we denote  $\rho_s(t)$

as  $\rho_s$ . Tracing out of the bath degrees of freedom in (A4) we obtain the following micromaser master like equation

$$\begin{aligned} \dot{\rho}_s = & -i[H_{\text{eff}}, \rho_s] + \frac{\mu}{2}\langle BB^\dagger \rangle \mathcal{L}[s]\rho_s + \frac{\mu}{2}\langle B^\dagger B \rangle \mathcal{L}[s^\dagger]\rho_s \\ & + \frac{\mu}{2}\langle B^2 \rangle \mathcal{L}_{\text{sq}}[s^\dagger]\rho_s + \frac{\mu}{2}\langle B^{\dagger 2} \rangle \mathcal{L}_{\text{sq}}[s]\rho_s, \end{aligned} \quad (\text{A5})$$

where  $\mu = p(\epsilon\tau)^2$  and  $H_{\text{eff}} = p\epsilon\tau(\langle B^\dagger \rangle s + \langle B \rangle s^\dagger)$ . The average values are taken with respect to the initial bath state, i.e.,  $\langle \mathcal{O} \rangle = \text{Tr}\{\rho_B(0)\mathcal{O}\}$ . The Lindblad superoperators are defined as:  $\mathcal{L}[o]\rho_s \equiv 2o\rho_s o^\dagger - o^\dagger o\rho_s - \rho_s o^\dagger o$  and  $\mathcal{L}_{\text{sq}}[o]\rho_s \equiv 2o\rho_s o - o^2\rho_s - \rho_s o^2$ . During the derivation of (A5) it was not necessary to specify if system  $S$  and/or  $B$  were from a bosonic or fermionic nature. Moreover, no restrictions have been made regarding their composition,  $S$  and  $B$  can represent either individual quantum systems or several non-interacting ones. As long as their interaction Hamiltonian can be written in the form of  $H_I$  together with the previous assumptions, (A5) will be valid.

It was assumed that between each random interaction the central system  $S$  evolves unitarily. However, it is possible that  $S$  could experience energy losses and/or decoherence during the evolution due to the unavoidable interaction with its surrounding. In such a case, it easy to prove (see Ref. [12]), within the approach of the theory of open quantum systems [43], that the only modification to (A5) is to add another series of Lindbladians,  $\propto \mathcal{L}_j[\mathcal{O}_j]\rho_s$ , for each  $j$  dissipation and/or dephasing process.

Equation (A5) reduces to Eq. (1) [Eq. (4)] choosing  $H_I$  as  $H_{\text{dip}}$  ( $H_{\text{TC}}$ ). In such case bath system  $B$  would be the non interacting  $N$ -qubit coherent cluster and we replace  $B$  by  $J_-$ . Central system  $S$  will be the single-qubit (single cavity field mode) so that  $s \rightarrow \sigma$  ( $a$ ) and  $\mu \rightarrow \mu_q$  ( $\mu_c$ ). Additionally, we demand that  $\rho_B(0)$  satisfy  $\langle B \rangle = \langle B^2 \rangle = 0$  while  $\langle B^\dagger B \rangle$  and  $\langle BB^\dagger \rangle$  should be different from zero. On the other hand, if we allow only  $\langle B \rangle$  and  $\langle B^\dagger \rangle$  to survive, just the unitary part of (A5) will remain, this is the condition to derive Eq. (17).

Eq. (A5) is quite general and it is applicable to several micromaser based models [7, 13, 14] including superradiant systems [9] and entangled qubit environments [51]. Also it works for the case of generalized quantum “phaseonium fuels” [10], where the bath system consists of a  $N + 1$  level atom with  $N$  degenerate coherent ground states [52]. Unlike those previous works, (A5) allows to get, more easily, analytical results.

### Appendix B: Autocorrelation functions

In the stationary case we know that  $\langle \sigma_+(0)\sigma_-(\tau) \rangle = \lim_{t \rightarrow \infty} \langle \sigma_+(t)\sigma_-(t + \tau) \rangle$  is the first order dipole-field ( $E^{(+)} \propto \sigma_-$ ) autocorrelation function in the steady state. The quantum regression formula (QRF) allows us to obtain such two-time correlation from the single-time function  $\langle \sigma_-(t) \rangle$  [43]. Identifying that  $\langle \sigma_-(t) \rangle = \rho_{eg}(t)$  and



$\langle\sigma_+(t)\sigma_-(t)\rangle = \rho_{ee}(t)$ , the use of the QRF in Eq. (2a) gives  $\langle\sigma_+(t)\sigma_-(t+\tau)\rangle = \rho_{ee}(t) \exp[-(2\gamma_\phi + (2t_q)^{-1})\tau]$ ; which in the steady state limit and in the Schrödinger picture yields

$$\langle\sigma_+(0)\sigma_-(\tau)\rangle = \rho_{ee}^{st} \exp[-(i\omega_q + 2\gamma_\phi + (2t_q)^{-1})\tau]. \quad (\text{B1})$$

For the time-dependent case, the solution for the den-

sity matrix is  $\rho_q(t) = U_q(t)\rho_q(0)U_q^\dagger(t)$ , where  $U_q(t) = \cos(t\Omega_{\text{eff}}/2) - i\sigma_x \sin(t\Omega_{\text{eff}}/2)$  [53]. Using  $U_q(t)$  the dipole-field autocorrelation function for the qubit, starting in its ground state  $\rho_q(0) = |g\rangle\langle g|$ , is

$$\begin{aligned} \langle g|\sigma_+(t_1)\sigma_-(t_2)|g\rangle &= \sin^2(t_1\Omega_{\text{eff}}/2) \sin^2(t_2\Omega_{\text{eff}}/2) \\ &+ \sin(t_1\Omega_{\text{eff}}) \sin(t_2\Omega_{\text{eff}})/4, \end{aligned} \quad (\text{B2})$$

which we use in the integral of Eq. (19) to obtain Eq. (20).

- 
- [1] Sai Vinjanampathy and Janet Anders, “Quantum thermodynamics,” *Contemporary Physics* **57**, 545–579 (2016).
  - [2] John Goold, Marcus Huber, Arnau Riera, Lidia del Rio, and Paul Skrzypczyk, “The role of quantum information in thermodynamics—a topical review,” *Journal of Physics A: Mathematical and Theoretical* **49**, 143001 (2016).
  - [3] Robert Alicki and Ronnie Kosloff, “Introduction to quantum thermodynamics: History and prospects,” in *Thermodynamics in the Quantum Regime: Fundamental Aspects and New Directions*, edited by Felix Binder, Luis A. Correa, Christian Gogolin, Janet Anders, and Gerardo Adesso (Springer International Publishing, Cham, 2018) pp. 1–33.
  - [4] Zeeya Merali, “The new thermodynamics: how quantum physics is bending the rules,” *Nature* **551**, 20–22 (2017).
  - [5] Marlan O. Scully, “Extracting work from a single heat bath via vanishing quantum coherence ii: Microscopic model,” *AIP Conference Proceedings* **643**, 83–91 (2002).
  - [6] Marlan O. Scully, M. Suhail Zubairy, Girish S. Agarwal, and Herbert Walther, “Extracting work from a single heat bath via vanishing quantum coherence,” *Science* **299**, 862–864 (2003).
  - [7] Ceren B. Da, Wolfgang Niedenzu, Fatih Ozaydin, zgr E. Mstecaplolu, and Gershon Kurizki, “Temperature control in dissipative cavities by entangled dimers,” *The Journal of Physical Chemistry C* **123**, 4035–4043 (2019).
  - [8] Angsar Manatuly, Wolfgang Niedenzu, Ricardo Roman-Ancheyta, Barıř akmak, zgur E. Mustecaphloęlu, and Gershon Kurizki, “Collectively enhanced thermalization via multiqubit collisions,” *Phys. Rev. E* **99**, 042145 (2019).
  - [9] Ali UC Hardal and zgur E. Mustecaphloęlu, “Superradiant quantum heat engine,” *Sci. Rep.* **5**, 12953 (2015).
  - [10] Deniz Turkpene and zgur E. Mustecaphloęlu, “Quantum fuel with multilevel atomic coherence for ultrahigh specific work in a photonic carnot engine,” *Phys. Rev. E* **93**, 012145 (2016).
  - [11] H. T. Quan, P. Zhang, and C. P. Sun, “Quantum-classical transition of photon-carnot engine induced by quantum decoherence,” *Phys. Rev. E* **73**, 036122 (2006).
  - [12] Jie-Qiao Liao, H. Dong, and C. P. Sun, “Single-particle machine for quantum thermalization,” *Phys. Rev. A* **81**, 052121 (2010).
  - [13] Ceren B. Daę, Wolfgang Niedenzu, zgur E. Mustecaphloęlu, and Gershon Kurizki, “Multiatom quantum coherences in micromasers as fuel for thermal and nonthermal machines,” *Entropy* **18**, 244 (2016).
  - [14] B. akmak, A. Manatuly, and . E. Mustecaphloęlu, “Thermal production, protection, and heat exchange of quantum coherences,” *Phys. Rev. A* **96**, 032117 (2017).
  - [15] J. Roßnagel, O. Abah, F. Schmidt-Kaler, K. Singer, and E. Lutz, “Nanoscale heat engine beyond the carnot limit,” *Phys. Rev. Lett.* **112**, 030602 (2014).
  - [16] Wolfgang Niedenzu, David Gelbwaser-Klimovsky, Abraham G. Kofman, and Gershon Kurizki, “On the operation of machines powered by quantum non-thermal baths,” *New Journal of Physics* **18**, 083012 (2016).
  - [17] Wolfgang Niedenzu, Victor Mukherjee, Arnab Ghosh, Abraham G. Kofman, and Gershon Kurizki, “Quantum engine efficiency bound beyond the second law of thermodynamics,” *Nature Communications* **9** (2018).
  - [18] Antonella De Pasquale and Thomas M. Stace, “Quantum thermometry,” in *Thermodynamics in the Quantum Regime*, edited by F. Binder, L. A. Correa, C. Gogolin, J. Anders, and G. Adesso (Springer, Berlin, 2018).
  - [19] Antonella De Pasquale, Davide Rossini, Rosario Fazio, and Vittorio Giovannetti, “Local quantum thermal susceptibility,” *Nature Communications* **7** (2016).
  - [20] Giacomo De Palma, Antonella De Pasquale, and Vittorio Giovannetti, “Universal locality of quantum thermal susceptibility,” *Phys. Rev. A* **95**, 052115 (2017).
  - [21] Antonella De Pasquale, Kazuya Yuasa, and Vittorio Giovannetti, “Estimating temperature via sequential measurements,” *Phys. Rev. A* **96**, 012316 (2017).
  - [22] Mohammad Mehboudi, Anna Sanpera, and Luis A. Correa, “Thermometry in the quantum regime: recent theoretical progress,” *Journal of Physics A: Mathematical and Theoretical* **52**, 303001 (2019).
  - [23] Sholeh Razavian, Claudia Benedetti, Matteo Bina, Yahya Akbari-Kourbolagh, and Matteo G. A. Paris, “Quantum thermometry by single-qubit dephasing,” *The European Physical Journal Plus* **134**, 284 (2019).
  - [24] Steve Campbell, Mohammad Mehboudi, Gabriele De Chiara, and Mauro Paternostro, “Global and local thermometry schemes in coupled quantum systems,” *New Journal of Physics* **19**, 103003 (2017).
  - [25] Steve Campbell, Marco G. Genoni, and Sebastian Deffner, “Precision thermometry and the quantum speed limit,” *Quantum Science and Technology* **3**, 025002 (2018).
  - [26] Luis A. Correa, Mohammad Mehboudi, Gerardo Adesso, and Anna Sanpera, “Individual quantum probes for optimal thermometry,” *Phys. Rev. Lett.* **114**, 220405 (2015).
  - [27] Patrick P. Hofer, Jonatan Bohr Brask, Martı Perarnau-Llobet, and Nicolas Brunner, “Quantum thermal machine as a thermometer,” *Phys. Rev. Lett.* **119**, 090603 (2017).

- (2017).
- [28] P. Filipowicz, J. Javanainen, and P. Meystre, “Theory of a microscopic maser,” *Phys. Rev. A* **34**, 3077–3087 (1986).
  - [29] Masashi Ban, “Decomposition formulas for  $su(1, 1)$  and  $su(2)$  lie algebras and their applications in quantum optics,” *J. Opt. Soc. Am. B* **10**, 1347–1359 (1993).
  - [30] Heinz-Peter Breuer, Francesco Petruccione, *et al.*, *The theory of open quantum systems* (Oxford University Press on Demand, 2002).
  - [31] C L Latune, I Sinayskiy, and F Petruccione, “Apparent temperature: demystifying the relation between quantum coherence, correlations, and heat flows,” *Quantum Science and Technology* **4**, 025005 (2019).
  - [32] Michael Tavis and Frederick W. Cummings, “Exact solution for an  $n$ -molecule—radiation-field hamiltonian,” *Phys. Rev.* **170**, 379–384 (1968).
  - [33] J. M. Fink, R. Bianchetti, M. Baur, M. Göppl, L. Steffen, S. Filipp, P. J. Leek, A. Blais, and A. Wallraff, “Dressed collective qubit states and the tavis-cummings model in circuit qed,” *Phys. Rev. Lett.* **103**, 083601 (2009).
  - [34] Ping Yang, Jan David Brehm, Juha Leppakangas, Lingzhen Guo, Michael Marthaler, Isabella Bovanter, Alexander Stehli, Tim Woltz, Alexey V. Ustinov, and Matrin Weides, “Probing the tavis-cummings level splitting with intermediate-scale superconducting circuits,” [arXiv:1810.00652](https://arxiv.org/abs/1810.00652) (2018).
  - [35] Marlan O. Scully and M. Suhail Zubairy, *Quantum Optics* (Cambridge University Press, 1997).
  - [36] Philipp Strasberg, Gernot Schaller, Tobias Brandes, and Massimiliano Esposito, “Quantum and information thermodynamics: A unifying framework based on repeated interactions,” *Phys. Rev. X* **7**, 021003 (2017).
  - [37] Andrei B Klimov and Sergei M Chumakov, *A group-theoretical approach to quantum optics* (John Wiley & Sons, 2009).
  - [38] Ronnie Kosloff, “Quantum thermodynamics: A dynamical viewpoint,” *Entropy* **15**, 2100–2128 (2013).
  - [39] William K. Wootters, “Entanglement of formation of an arbitrary state of two qubits,” *Phys. Rev. Lett.* **80**, 2245–2248 (1998).
  - [40] T. Baumgratz, M. Cramer, and M. B. Plenio, “Quantifying coherence,” *Phys. Rev. Lett.* **113**, 140401 (2014).
  - [41] Norbert Wiener, “Generalized harmonic analysis,” *Acta Math.* **55**, 117–258 (1930).
  - [42] Alexander Khintchine, “Korrelationstheorie der stationären stochastischen prozesse,” *Mathematische Annalen* **109**, 604–615 (1934).
  - [43] Howard Carmichael, *An open systems approach to quantum optics*, Vol. 18 (Springer Science & Business Media, 1993) p. 41.
  - [44] Héctor M. Castro-Beltrán, Ricardo Román-Ancheyta, and Luis Gutiérrez, “Phase-dependent fluctuations of intermittent resonance fluorescence,” *Phys. Rev. A* **93**, 033801 (2016).
  - [45] J. H. Eberly and K. Wódkiewicz, “The time-dependent physical spectrum of light\*,” *J. Opt. Soc. Am.* **67**, 1252–1261 (1977).
  - [46] R. Román-Ancheyta, O. de los Santos-Sánchez, L. Horvath, and H. M. Castro-Beltrán, “Time-dependent spectra of a three-level atom in the presence of electron shelving,” *Phys. Rev. A* **98**, 013820 (2018).
  - [47] B. R. Mollow, “Power spectrum of light scattered by two-level systems,” *Phys. Rev.* **188**, 1969–1975 (1969).
  - [48] D. Meschede, H. Walther, and G. Müller, “One-atom maser,” *Phys. Rev. Lett.* **54**, 551–554 (1985).
  - [49] Gerhard Rempe, Herbert Walther, and Norbert Klein, “Observation of quantum collapse and revival in a one-atom maser,” *Phys. Rev. Lett.* **58**, 353–356 (1987).
  - [50] G. Rempe, F. Schmidt-Kaler, and H. Walther, “Observation of sub-poissonian photon statistics in a micromaser,” *Phys. Rev. Lett.* **64**, 2783–2786 (1990).
  - [51] Shakib Daryanoosh, Ben Q. Baragiola, Thomas Guff, and Alexei Gilchrist, “Quantum master equations for entangled qubit environments,” *Phys. Rev. A* **98**, 062104 (2018).
  - [52] Deniz Türkpençe and Ricardo Román-Ancheyta, “Tailoring the thermalization time of a cavity field using distinct atomic reservoirs,” *J. Opt. Soc. Am. B* **36**, 1252–1259 (2019).
  - [53] R. Juárez-Amaro, Arturo Zuñiga-Segundo, and HM Moya-Cessa, “Several ways to solve the jaynes-cummings model,” *Appl. Math. Inf. Sci.* **9**, 299 (2015).